ISTITUTO NAZIONALE DI RICERCA METROLOGICA
Repository Istituzionale

Nonsilica Oxide Glass Fiber Laser Sources: Part I

(Article begins on next page)

28 April 2024

We are IntechOpen,
the world's leading publisher of
Open Access books
Built by scientists, for scientists

4,200
Open access books available

116,000
International authors and editors

125M
Downloads

Our authors are among the

154
Countries delivered to

TOP 1%
most cited scientists

12.2%
Contributors from top 500 universities

CLARIVATE ANALYTICS
BOOK
CITATION
INDEX
INDEXED

WEB OF SCIENCE™

Selection of our books indexed in the Book Citation Index
in Web of Science™ Core Collection (BKCI)

Interested in publishing with us?
Contact book.department@intechopen.com

Nonsilica Oxide Glass Fiber Laser Sources: Part I

Daniel Milanese, Joris Lousteau, Xiushan Zhu,
Arturo Chavez-Pirson, Diego Pugliese,
Nadia Giovanna Boetti and Nasser Peyghambarian

Additional information is available at the end of the chapter

Abstract

Nonsilica oxide glasses have been developed and studied for many years as promising alternatives to the most used silica glass for the development of optical fiber lasers with unique features and properties. Depending on the glass former of choice, these glasses can offer very distinctive physical properties if compared to silica-based glasses. With regard to the development of photonic fiber devices, these key properties include low phonon energy, high rare-earth ion solubility, high optical nonlinearity and easy handling procedures. This chapter, part I of a detailed study concerning nonsilica oxide glass–based optical fiber laser sources, reviews the main properties of three different nonsilica oxide glass families, namely phosphate, germanate and tellurite. The manufacturing process of an optical fiber using these glass materials is also discussed in Section 3 of this chapter.

Keywords: nonsilica oxide glass, phosphate glass, germanate glass, tellurite glass, rare-earth–doped optical fiber, fiber laser, built-in-casting, suction casting, rod-in-tube, rotational casting

1. Introduction

Inorganic glasses have been playing a key role in the development of optical devices and instruments, thanks to the unique combination of different properties: they are transparent in the visible region, mechanically stiff and resistant, chemically durable and can be easily manufactured into different highly homogenous forms and sizes. Starting from ancient times, transparent glasses were fabricated to make windows and goblets, then later, thanks to the improvement in the glass manufacture brought about by Venetian masters in the Middle Age, stable glass compositions were processed into eyeglasses, lenses and mirrors. High-quality

optical glasses became key player materials for the fabrication of lenses for telescopes and microscopes, thus enabling tremendous development of modern science [1]. Finally, long haul optical fiber–based backbone networks are based on extremely pure and low loss glasses, which then are enabling materials for the internet revolution [2, 3].

Due to their outstanding ultra-low propagation loss and intrinsic thermomechanical properties, silica-based glasses have been the material of choice for most optical fiber–related applications. As passive media, they were crucial in allowing the deployment of long haul fiber networks and found applications even as nonlinear frequency conversion fiber laser sources, despite the low intrinsic nonlinearity of silica. When doped with rare-earth (RE) ions, they have been used for fiber lasers and amplifiers with outstanding performance in the near-infrared wavelength region [4].

Despite its success, however, silica glass possesses several intrinsic limits:

1. The high phonon energy of silica glass around 1100 cm^{-1} [5] permits to exploit only a restricted range of the possible emission wavelengths offered by RE ions. Silica glass fibers have proved to be outstanding for the development of 1, 1.5 and 2 μm laser sources, but numerous applications require alternative wavelengths, in particular in the mid-infrared (mid-IR) wavelength region.

2. The RE doping concentration level is limited in silica glass [6]: both the nature of the silica glass network and the doping process itself limit the doping concentration achievable. Thus, silica glass cannot be used to develop short-length devices that are required for a single-frequency fiber laser and for the development of low-nonlinearity booster amplifier for high peak power lasers.

3. Additionally, the short infrared transmission edge of silica glasses restricts their use for numerous high-impact applications, such as mid-IR laser, chemical sensing and infrared imaging [7].

The so-called soft glasses are based on alternative glass formers exhibiting different nature and structure, which offer alternative phonon energies and transmission characteristics, high RE ion doping levels (up to 10^{21} ions/cm^3) and high optical nonlinearity (orders of magnitude higher than that exhibited by silica glass). Soft glasses include oxide and nonoxide glasses. Nonoxide glass compositions of great interest for laser emission in the mid-IR wavelength region are mainly based on fluoride [8] and chalcogenide [9, 10] glass formers. They provide a wide transmission window extending up to the mid-IR well above 2 μm, but their low chemical stability and poor mechanical properties have so far strongly limited their use for devices in harsh environment. Oxide glasses, although exhibiting shorter wavelength range of operation in the infrared, are suitable for the integration with commercial fiber–based components and demonstrated reliability for the incorporation in operational environment.

In this chapter, we present a detailed overview of the most promising oxide-based soft glass systems, namely phosphate, germanate and tellurite, together with the fabrication of fibers based on these glass families. The synthesis and individual physical properties of these glasses are presented in Section 2 to identify their prospect and range of applications. The engineering

techniques used to manufacture optical fiber preforms out of these glasses and the fiber drawing are then discussed in Section 3.

2. Nonsilica oxide glasses

Engineering a glass for a specific photonic application requires the knowledge of some key parameters that enable its use. In reviewing the main oxide glass system alternative to silica-based compositions, we will focus on the following properties: solubility of RE ions, chemical durability, thermal stability, mechanical reliability, ease of fabrication, fiber drawing ability, nonlinearity and phonon energy. This last property is less familiar outside the community of glass scientists working on active materials for lasers. In studying a suitable material for coherent sources in the mid-IR, a particular effort is required to design hosts that minimize their interaction with the electronic transitions of the ions leading to the emission of photons. High phonon energy glasses cause the decay from an excited state to a lower state to occur via nonradiative emission of heat, in the form of phonons, thus decreasing the overall efficiency of the laser emission [4]. In this section, these properties of phosphate, germanate and tellurite glasses are reviewed.

Table 1 lists the main physical properties of the phosphate, germanate and tellurite glasses reviewed in this chapter and their values compared with silica-based glass [11–18].

2.1. Synthesis of nonsilica oxide glasses

The synthesis of silica glass has been subjected to continuous evolution, with the aim of reducing the causes of extrinsic absorption due to the presence of impurities, namely transition

Glass system	Silica	Phosphate	Germanate	Tellurite
Transmission range (μm)	0.2–2.5	0.2–4.3	0.3–4.0	0.4–5.0
Maximum phonon energy (cm^{-1})	1100	1200	975	800
Glass transition temperature (°C)	1200	400–550	400–450	300–350
Thermal conductivity ($Wm^{-1}K^{-1}$)	1.38	0.57	0.70	1.25
Expansion coefficient (10^{-6}/K)	0.55	13.40	8–11	12–17
Density (g/cm^3)	2.2	2.6	3 ÷ 7.2	5.5
Young's modulus (GPa)	70	47	65	33.6
Refractive index @1.55 μm	1.45	1.56	1.63	1.8–2.3
Abbe number	80	44–82	15–41	10–20
Nonlinear refractive index (m^2/W)	10^{-20}	10^{-20}	10^{-20}	2.5×10^{-19}
Fiber loss (dB/Km)	0.2 @ 1.55 μm	1.5×10^3 @ 1.05 μm	1.2×10^3 @ 1.2 μm	200 @ 1.2 μm
RE solubility (ions/cm^3)	10^{19}	10^{21}	10^{21}	10^{21}

Table 1. Main properties of nonsilica oxide glass systems.

metal ions and water. This led to the development of chemical vapor deposition methods: these synthesis routes utilize chemical precursors in vapor phase as starting reagents, which are transformed into the final oxide components by reaction with oxygen at very high temperatures. These techniques allowed the fabrication of optical fibers capable of providing <0.2 dB/km ultra-low loss in the third telecom window.

Chemical precursors involved in the synthesis of multicomponent nonsilica oxide glasses have very distinct vapor pressures, making high-purity vapor-based fabrication techniques unsuitable for this type of glass compositions. Instead, traditional glass melting techniques must be implemented. Chemical precursors are weighed and batched into a crucible typically made of alumina, silica or a noble metal such as Pt or Au. The glass batch is then melted in a high-temperature furnace for few hours under controlled atmosphere. Typical melting temperatures for the glasses under consideration in this chapter are 800, 1200 and 1300°C for tellurite, germanate and phosphate glasses, respectively. Because of the corrosive nature of some of the chemical precursors involved, this melt casting process leads to an inevitable degree of optical contamination, both related to the initial purity of the chemical precursors but also to possible cross-contamination occurring through the whole preparation process. Crucible material is of prime importance, as some degree of dissolution in the glass can occur during the melting process [19]. Although the final glass material produced through this process does not compete with the purity of standard silica glass preform, yet optical losses below 100 dB/km are readily achievable under meticulous and clean melting conditions.

Moreover, the melt casting process provides the advantage that the glass can be easily shaped using adequate casting mold geometry. This feature is largely exploited when preparing multicomponent glass preforms, as discussed in the following paragraphs.

2.2. Phosphate glasses

Pure phosphate glasses have not been historically as popular as silicate glasses, because of their poor chemical stability and mechanical properties [20], which, however, could be significantly improved by the addition of proper modifier and intermediate ions [21, 22]. Phosphate glasses were mainly used for HF-resistant glasses and for other niche applications [20]. Later on, research works on phosphate glasses were stimulated by the wide range of potential and commercial applications of these materials, from the treatment of hard-water [23] to biomedicine [24] and for the storage of radioactive wastes [25].

Optical quality phosphate glasses, initially developed by Schott and coworkers, were of interest also for their UV transparency [26], but found no significant applications due to their poor stability. However, the need of a suitable gain medium for high-peak power lasers such as the one developed within the framework of the inertial confinement fusion (ICF) research led to a resurge in their employment, after careful engineering of the compositions [27].

2.2.1. Structure

The basic units that constitute the phosphate glass are the P-tetrahedra, with a central phosphorous atom surrounded by four oxygen atoms. These are connected through bridging

oxygen (BO) atoms to give different phosphate anions. The tetrahedra are classified using the Q^i terminology [28], where 'i' represents the number of tetrahedra linked to the unit (shown schematically in **Figure 1**).

Depending on the oxygen to phosphorous ratio, phosphate glasses can be classified into a series of subcategories, from ultra-phosphate (O/P ≤ 3) to ortho-phosphate (O/P = 4).

The O/P ratio in vitreous phosphate (v-P_2O_5) is derived from the stoichiometry of the pure compound and it is equal to 2.5. The basic unit of the structure of the v-P_2O_5 is the Q^3 tetrahedron, which has three covalent bonds via BO atoms with the neighbor tetrahedra and a terminal shorter bond via nonbridging oxygen (NBO) atoms.

The structural strength and chemical durability of the optical phosphate glass can be improved by adding appropriate components, as described in several patents and papers [29–31]. Metal oxides added to v-P_2O_5 can improve the physical properties and chemical stability of the system. In more detail, alkali metal oxides R_2O (R = Li, Na, K, Rb and Cs) can be added to the glass to increase the RE solubility [32]. Network intermediates R_2O_3 (R = B and/or Al) are also added in phosphate glasses to improve their chemical durability and mechanical properties and to decrease the solubility in water. If the amount of R_2O_3 is too low, the glass is water soluble, while if the amount of R_2O_3 is too high, an increase in the glass transition temperature (T_g) and the crystallization temperature occurs [33]. In particular, even a small addition of R_2O_3 can significantly improve the mechanical properties of the phosphate glass. This is due to the particular behavior of R^{3+} ions that can have both tetrahedral and trigonal coordination [33–35]. The presence of alkali-earth oxide MO (M = Mg, Ca, Ba, Sr and Zn) in the glass prevents the devitrification and improves the chemical durability [35]. When the amount of MO is too low, the glass is hygroscopic and has poor chemical durability and poor optical quality; when the amount of MO is too high, the glass tends to devitrify [29].

In conclusion, the addition of various dopants, such as alumina, alkali and earth-alkali oxides, was demonstrated to reinforce the phosphate glass network. Moreover, when RE ions were added, the glasses proved to be suitable materials for lasers, showing an interesting combination of low nonlinear refractive index and high optical gain.

2.2.2. Phosphate glasses as laser material

Phosphate glasses doped with Nd^{3+} ions have proved suitable for the fabrication of large monolithic active material sections constituting the high-peak power laser at Lawrence
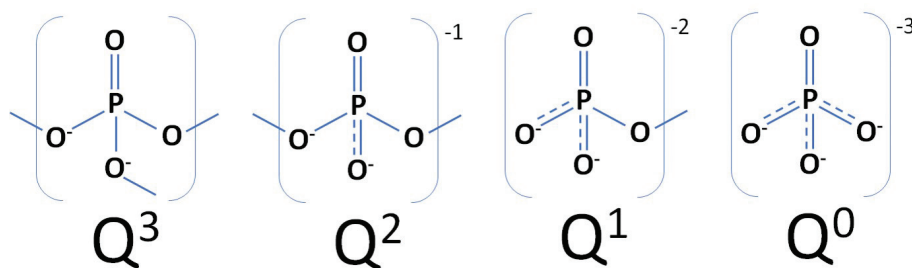

Figure 1. Types of tetrahedral sites occurring in phosphate glasses depending on their composition.

Livermore Laboratories and in other laser ignition facility infrastructures around the world [27]. This was possible by developing compositions with high durability, which displayed a high-emission cross-section, low nonlinear refractive index and high energy storage and extraction characteristics [36]. Besides, phosphate glasses, with respect to silicate glasses, can be fabricated free of Pt inclusions, which may cause catastrophic damage to the optical active material [37].

More recently, the development of high-peak pulsed optical amplifiers asked for materials able to incorporate high amounts of RE ions, and phosphate glasses became an ideal candidate since up to 10^{21} ions/cm^3 of RE can be accommodated without clustering effects [38]. This is important for pulsed optical amplifiers, where nonlinear optical effects must be minimized: phosphate glass allows reducing the length of the amplifier with respect to the silica counterpart. In addition, phosphate glasses are also less susceptible than silica to photodarkening [39] and display cross-sections.

Finally, their mechanical reliability allows the integration of phosphate fibers with commercial silica fibers through cleaving and arc fusion splicing [40].

Phosphate glasses used for lasers in the eye-safe wavelength region usually incorporate erbium (Er^{3+}) as activator ion, with emission centered at around 1550 nm corresponding to the radiative decay from the $^4I_{13/2}$ excited state to the ground state $^4I_{15/2}$ (see **Figure 2**). Like in the case of
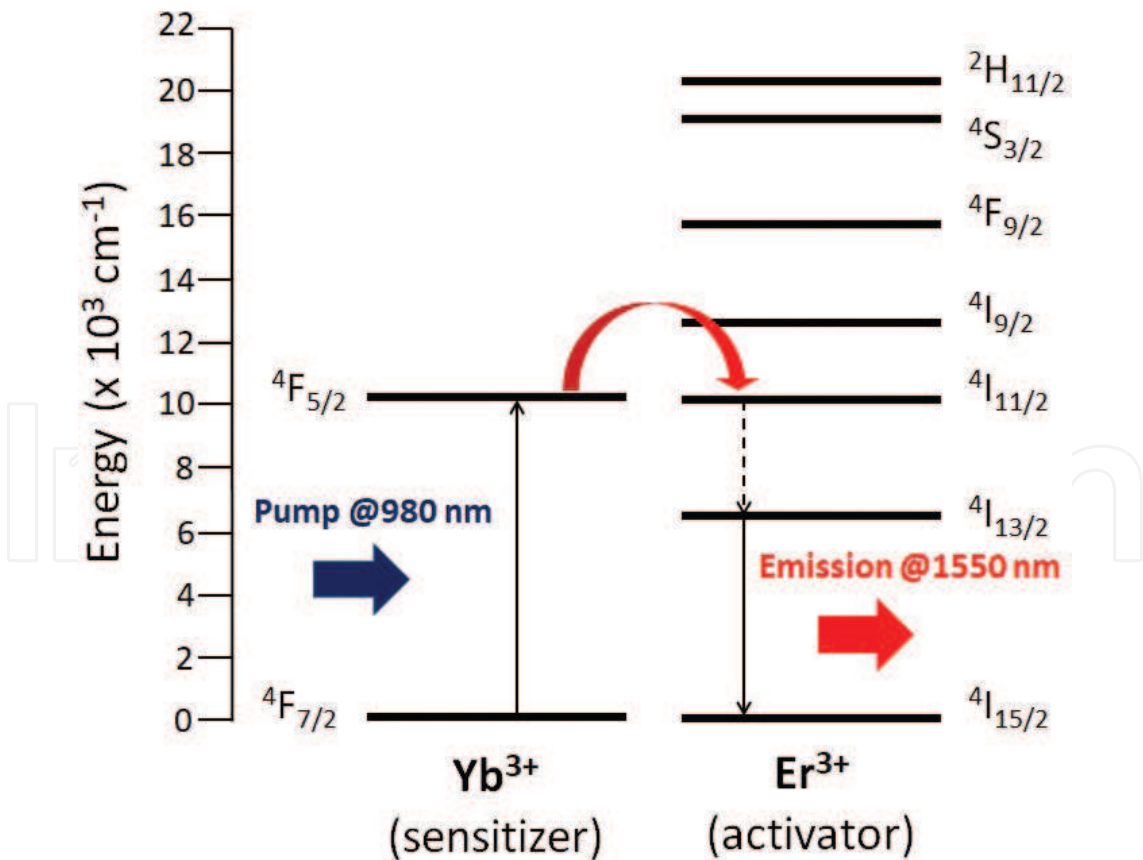

Figure 2. Energy level diagrams of Yb^{3+} and Er^{3+} ions. The main pumping mechanism of the sensitizer-activator scheme is also reported.

Nd^{3+}, also the cross-section of Er^{3+} ions in phosphate host is high: values at peak of around 7.0×10^{-21} cm^2 are reported with respect to values of around 5.5×10^{-21} cm^2 for silica [4, 41]. In order to improve the overall efficiency of the lasing process, ytterbium (Yb^{3+}) ions are often employed as sensitizer in combination with Er^{3+} ions: thanks to the superior absorption cross-section at the pump wavelength (980 nm) of these ions, the excitation from the ground state $^2F_{7/2}$ to the $^2F_{5/2}$ excited state takes place. The energy is then transferred to the $^4I_{11/2}$ excited state of erbium, which decays through the nonradiative $^4I_{11/2} \rightarrow {}^4I_{13/2}$ transition followed by the radiative transition $^4I_{13/2} \rightarrow {}^4I_{15/2}$. This energy transfer reduces the threshold of the laser emission and improves the efficiency of the device [42, 43]. The interplay between ytterbium and erbium ions is depicted in **Figure 2**. Phosphate glass represents, with respect to silica, an ideal host because its high phonon energy allows obtaining transfer efficiencies up to 95% [44].

The lifetime values of the excited state corresponding to the upper laser level provide useful indications of the population inversion ability of the emitter. A higher lifetime value is preferred because that will allow the large population inversion needed for high gain and low noise optical amplifiers. In the case of lasers, high lifetime values will permit lower pump power to reach the laser threshold, with resulting higher efficiency in laser emission and lower heat accumulation in the material. Silica, given the lower oscillator strength of the $^4I_{13/2} \rightarrow {}^4I_{15/2}$ transition, displays generally a higher lifetime value (10.80 ms) than phosphate glass (8.25 ms) [4]. However, phosphate glasses maintain high lifetime values even for high erbium concentrations: values of 7.5 ms are reported for an erbium concentration of 6×10^{20} $ions/cm^3$ [45].

2.3. Germanate glasses

Pure germanium oxide was obtained in its glassy state around 90 years ago [19], showing similar properties to silica in terms of mechanical strength and chemical stability, although the high cost of the raw materials did not make it an attractive alternative. However, since the Ge—O bond displays a lower energy than Si—O, germanate glasses present a shift to lower wavenumbers in their phonon energy with respect to silica from 1100 to 900 cm^{-1}, thus extending the transparency window up to 4.5 μm [46]. GeO_2 glass was thus proposed as optically transparent material alternative to silica for telecom applications, thanks to the intrinsically low attenuation at the wavelength of 2 μm [47]. Lead germanate glasses [48] were developed and studied in the view of laser beam delivery above 1.5 μm [49]. RE–doped alkali germanate glasses were explored as magneto-optic materials: Faraday angle rotation was measured, providing a linear variation of Verdet constant with the concentration of RE ions [50].

2.3.1. Structure

The structural units of pure germanium dioxide glass are GeO_4 tetrahedra. Binary alkali germanate glasses undergo a change from 4-fold Ge to 6-fold Ge (GeO_6 octahedra), with a corresponding increase in density and refractive index, which reaches a maximum at around 15 mol% of M_2O modifier. Higher values of modifier produce a progressive formation of 4-fold coordinated Ge accompanied by a gradual depolymerization of the network through an increase of nonbridging oxygens. This behavior is also known as the "germanate anomaly" [51, 52].

Lead germanate glasses are made of a mixture of 4- and 6-fold coordinated Ge, which, with increasing the doping level of lead, turns into a predominance of GeO_4 tetrahedral units.

These characteristics, together with high RE solubility, make them very interesting for the development of laser devices operating above 1.5 μm.

2.3.2. Germanate glasses as laser material

Germanate glasses, among oxide soft glasses, are the best in terms of mechanical properties, thanks to the great similarity of GeO_2 with SiO_2. Lead germanate glasses show an outstanding resistance to devitrification [53] and a wide transmission window, while offering a suitable environment for RE ions, thanks to the low phonon energy of 920 cm^{-1}.

For the above-mentioned reasons, the main studies of germanate glasses were focused on those RE ions emitting at wavelengths above 1.5 μm, namely Tm^{3+}, Ho^{3+} and Er^{3+}.

Tm^{3+} ions are of interest for the emission in the mid-IR wavelength region at around 2 μm. A maximum output power of 346 mW and a slope efficiency of 25.6% were obtained when pumping a 1 mol% Tm-doped germanate glass by a 790 nm laser diode [54]. The glass was characterized by good forming ability and chemical durability and exhibited a large emission cross-section of 8.69×10^{-21} cm^2, a high quantum efficiency of the Tm^{3+}: $^3F_4$ level of 71% and a low nonradiative relaxation rate of the $^3F_4 \rightarrow {}^3H_6$ transition of 0.09 ms^{-1}.

In view of enhancing the intensity of the 1.8 μm emission of Tm^{3+} ions, the Yb^{3+} ion codoping is commonly adopted due to the large absorption of Yb^{3+} at the diode-pumping wavelength of 980 nm. Among the interesting sensitizers, Yb^{3+} presents the advantage of displaying a simple energy level scheme, which is beneficial for obtaining large absorption and emission cross-sections and for avoiding any undesirable excited state absorption under intense pumping [55]. The radiative characteristics and spectroscopic properties of Yb^{3+}/Tm^{3+}-codoped bismuth germanate glasses with different concentrations of Yb_2O_3 were thoroughly investigated under the excitation of a conventional 980 nm laser diode [56]. The efficient sensitization of Tm^{3+} ions with Yb^{3+} ions was proved by the larger energy transfer coefficient (4.81×10^{-40} cm^6/s) and higher energy transfer efficiency (89%) from Yb^{3+} to Tm^{3+} ions. Moreover, a noticeable peak emission cross-section value of 7.66×10^{-21} cm^2 was calculated based on the emission spectrum.

It is worthwhile noting, however, that the intense upconversion emissions at 480 and 800 nm generated by the strong excited state absorption in the Tm^{3+}/Yb^{3+}-codoped glasses [57] and the lack of flexible pump sources make the sensitization of Tm^{3+} ions with Yb^{3+} ions not always advantageous. To overcome these drawbacks, transition metal (TM) Cr^{3+} ions have been successfully employed as a sensitizer for their two intensive and broad absorption bands from ultraviolet to near-infrared range, which offer a variety of selective pump wavelengths. An enhanced 1.8 μm emission band of Tm^{3+}: $^3F_4 \rightarrow {}^3H_6$ in an extremely extended excitation band of 380–900 nm was obtained in fluorogermanate glasses through strong sensitization of Cr^{3+} when pumped by an 808 nm laser diode [58]. An energy transfer efficiency from Cr^{3+} to Tm^{3+} as high as 91.10% was calculated based on experimental data, thus proving that these Cr^{3+}/Tm^{3+}-codoped fluoro-germanate glasses are promising matrices for applications in near-infrared eye-safe fiber lasers and amplifiers.
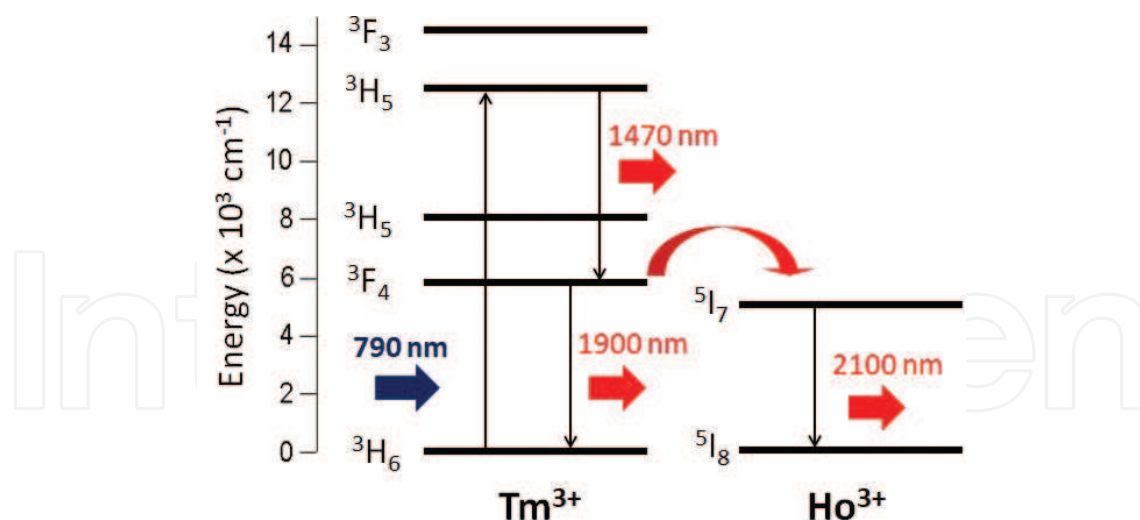
Figure 3. Energy levels of Tm^{3+} and Ho^{3+} ions of interest for the emission in the mid-IR wavelength region.

Besides Tm^{3+}, other promising RE ions in pursuit of the fabrication of high-power and efficient laser sources in the wavelength region around 2 μm are the Ho^{3+} ions. The energy levels of the two ions are reported in **Figure 3**. The emission cross-section of Ho^{3+} is about five times higher than that of Tm^{3+} and, in addition, the fluorescence lifetime of Ho^{3+} is promising in view of developing Q-switched lasers [59]. Unlike Tm^{3+}, Ho^{3+} cannot be pumped directly by using the common commercially available laser diodes operating at 808 or 980 nm for the lack of a suitable absorption band. One intriguing approach to overcome this issue consists in the sensitization of Ho^{3+} ions with other RE ions exhibiting strong absorption bands near the wavelength of existing commercial laser diodes, such as Yb^{3+}, which displays strong absorption bands near 980 nm.

The 2 μm emission properties and energy transfer processes of Ho^{3+}-doped germanate glasses sensitized by up to 12 mol% of Yb^{3+} were deeply investigated with the purpose of manufacturing a near-infrared eye-safe solid-state laser [60]. The emission cross-section of the Ho^{3+}: $^5I_7 \rightarrow {}^5I_8$ transition near 2 μm was 8.6×10^{-21} cm^3, and the coefficient of the forward energy transfer (Yb^{3+}: $^2F_{5/2} \rightarrow Ho^{3+}$: $^5I_7$) revealed to be 19 times larger than that of the backward transfer (Yb^{3+}: $^2F_{5/2} \leftarrow Ho^{3+}$: $^5I_7$). Interestingly, the glass codoped with 5.0 mol% Yb_2O_3 and 1.0 mol% Ho_2O_3 displayed the highest gain in the 2 μm region.

The mid-infrared emission properties at around 2.85 μm in Ho^{3+}/Yb^{3+}-codoped germanate glasses characterized by a noticeably low OH^- absorption coefficient of 0.24 cm^{-1} and also by a low phonon energy equal to 790 cm^{-1} were reported [61]. The glasses exhibited a large spontaneous transition probability of 36.66 s^{-1}, corresponding to the Ho^{3+}: $^5I_6 \rightarrow {}^5I_7$ transition, and a broad 2.85 μm fluorescence. Moreover, a peak emission cross-section of 9.2×10^{-21} cm^2 and a predicted maximum gain per unit length at 2.85 μm of 4.3 dB/cm were achieved.

Another interesting research work thoroughly investigated the 2.05 μm emission of Ho^{3+}: $^5I_7 \rightarrow {}^5I_8$ and the energy transfer mechanisms of Ho^{3+} sensitized by Tm^{3+} and Er^{3+} in novel Ho_2O_3, Tm_2O_3 and Er_2O_3 triply doped germanate glasses [62]. The maximum value of

emission cross-section of Ho^{3+} at around 2.05 μm proved to be 8.003×10^{-21} cm^2, and a noticeable enhancement in the 2.05 μm emission of Ho^{3+}: $^5I_7 \rightarrow {}^5I_8$ was observed when adding the proper amount of Er_2O_3 and Tm_2O_3 under excitation at 808 nm. The maximum value of the Ho^{3+} 2.05 μm emission intensity was obtained at concentrations of Ho_2O_3, Tm_2O_3 and Er_2O_3 equal to 1, 1 and 2 mol%, respectively.

Among the different RE ions able to efficiently emit in the mid-IR wavelength region, a prominent role is played by Er^{3+}, which is an ideal luminescent center for the 2.7 μm emission corresponding to the $^4I_{11/2} \rightarrow {}^4I_{13/2}$ transition and can be directly pumped by using the commercially available and low-cost 808 or 980 nm laser diodes.

For the above-mentioned transition, high spontaneous radiative transition probability of 30.09 s^{-1}, large emission cross-section equal to $(14.84 \pm 0.10) \times 10^{-21}$ cm^2 and superior gain performance were obtained from 1 mol% Er^{3+} activated germanate glasses characterized by good forming ability and thermal stability [63]. Moreover, La_2O_3 and Y_2O_3 modified 1 mol% Er^{3+}-doped germanate glasses with good thermal stability were also synthesized, and their peak emission cross-sections corresponding to the $^4I_{11/2} \rightarrow {}^4I_{13/2}$ transition revealed to be $(14.3 \pm 0.10) \times 10^{-21}$ cm^2 and $(15.4 \pm 0.10) \times 10^{-21}$ cm^2, respectively [64].

2.4. Tellurite glasses

TeO_2 cannot form a noncrystalline solid if quenched rapidly, since the compound does not obey the Zachariasen's rules for glass forming [65]. More stable glasses are obtained when a modifier ion is added, such as BaO, ZnO or Na_2O, the first discovery of glass formation dating back to Berzelius in 1834 [19]. Tellurite glasses have been studied and developed mainly for photonic applications: they offer an interesting alternative to silica mainly because of their high refractive index, good chemical stability and the lowest phonon energy among oxide glasses [12]. They were initially investigated for their potential use as optical amplifiers in the third telecom window. They represent a valid alternative to fluoride glasses as host materials for Tm^{3+} ions operating at the wavelength of 1.47 μm, as part of the thulium-doped fiber amplifier (TDFA). Indeed, tellurite glasses display a wider bandwidth, better depopulation of $^3F_4$ level and higher absorption and emission cross-sections, which increase the efficiency of the amplification [66]. Another interesting feature of tellurite glasses, unique among oxide glasses, is their high refractive index, which opens perspectives for the use of these materials for supercontinuum generation in the mid-IR wavelength region [67]. Faraday angle rotation using both passive and RE–doped tellurite glasses has also been investigated [68].

2.4.1. Structure

Tellurium oxide–based glasses are structured into a predominance of TeO_4 units in trigonal bipyramid arrangement (4-fold coordinated Te, sp^{3}d hybridization), which with the addition of modifier ions change into TeO_3 trigonal pyramids (3-fold coordinated Te, sp^3 hybridization). An intermediate structure of TeO_{3+1} polyhedron was also detected using several types of spectroscopic techniques [69, 70].
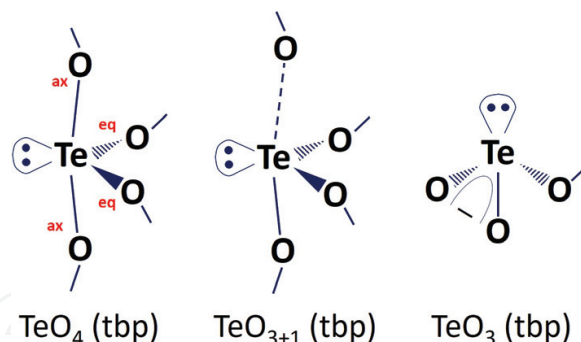
Figure 4. TeO_4, TeO_{3+1} and TeO_3 structural units typical of tellurite glasses.

In tellurite glasses, the TeO_4 trigonal bipyramid (tbp) structural units contain two axial oxygen atoms (O_{ax}) at a distance of 191 pm from the Te atom and two equatorial oxygen atoms (O_{eq}) at the distance of 209 pm. The angles between O_{ax}—Te—O_{ax} and O_{eq}—Te—O_{eq} atoms are 169 and 102°, respectively. With the addition of glass modifiers, the Te—O_{ax} bonds become weaker and longer, which causes the structural change of some TeO_4 units into TeO_{3+1} units and, in a following step, with increasing the amount of glass modifiers, into TeO_3 units. The different structural units are reported in **Figure 4**. Such process is caused by the electron transfer from the glass modifier to a more electronegative $(TeO_4)4\delta$ (where $0 < \delta < 1$ is a parameter representing the ionic character of the Te—O bond) unit [71, 72].

2.4.2. Tellurite glasses as laser material

Tellurite glass has been studied for laser emission since 1978, when the first Nd-doped bulk glass laser was demonstrated [73] by exciting it at the Ar-ion laser emission wavelength of 514.5 nm.

Among oxide glass systems, tellurite glasses are a promising glass host for near-IR and mid-IR lasers thanks to their peculiar properties. The high RE ion solubility (up to ~10^{21} ions/cm^3) within its amorphous matrix allows the realization of highly compact devices. Moreover, tellurite glasses display the lowest phonon energy among all oxide glasses (in the range of 650–800 cm^{-1} depending on the composition), which allows transmission further into the infrared (up to ~5 μm), and high refractive index (~2.0), which means high absorption and emission cross-sections [74, 75]. Tellurite glasses are also more chemically, environmentally and thermally stable than other nonoxide glasses, making them an attractive option for reliable fiber device manufacturing [12].

A drawback of tellurite glasses, like most oxide glasses fabricated from solid-state precursor materials, is the presence of hydroxyl ions (OH$^-$), which absorb in the mid-IR wavelength region. These ions could decrease the fluorescence intensity and ultimately lead to the deterioration of the laser performance and even inhibit the laser output [75]. In the tellurite glass system, significant results of RE ion emission in the mid-IR region have been reported from Tm^{3+}, Ho^{3+} and Er^{3+} [76–82].

Thulium (Tm) is an ideal choice for the realization of glass lasers in the ~2 μm wavelength range, since it displays one of the broadest fluorescence bands among RE ions [83] due to the transition $Tm^{3+}: {}^3F_4 \rightarrow {}^3H_6$ that is centered at around 1.8 μm. Tm^{3+} has also the advantage of having an absorption band conveniently located at around 800 nm, which coincides with the output of low-cost and high-power commercial laser diodes. This pumping scheme allows obtaining two ions in the upper laser level for each pumping photon, thanks to a phonon-assisted cross-relaxation process that can potentially result in a laser action with 200% quantum efficiency [84, 85]. It is possible also to pump Tm^{3+} directly into the upper laser level ${}^3F_4$, which has the potential benefit of a low quantum defect, but has the disadvantage of the lack of convenient low-cost and high-power sources operating in this wavelength range. Possible options that have been demonstrated are an Er^{3+}/Yb^{3+}-codoped tellurite fiber laser [84] and low-power semiconductor laser diodes [86].

Spectroscopic properties of Tm^{3+}-doped TZN (80 TeO_2-10 ZnO-10 Na_2O) and TZNG (75 TeO_2-10 ZnO-10 Na_2O-5 GeO_2) glasses were reported and studied in [76]. The measured full width at half maximum (FWHM) of the $Tm^{3+}:{}^3F_4$ fluorescence band in TZN glass was 200 μm, compared to 125 nm reported in ZBLAN [87] and 150 nm in silica [88], thus resulting in an enhanced tuning range obtainable in tellurite glass host material. In this work, lasing was also demonstrated in TZNG bulk glass pumped at 793 nm by a Ti:sapphire laser, with a maximum output power of 124 mW and a slope efficiency of 28% with respect to the absorbed pump power. In order to enhance the quantum yield of Tm^{3+} 1.8 μm emission, codoping with Yb^{3+} was proposed [89–91] due to its efficient absorption at 980 nm, which is readily available from InGaAs laser diodes. Moreover, the simple energy level structure of the ytterbium ion offers also an additional benefit by avoiding undesirable excited state absorption (ESA). In [89], an efficient energy transfer between Yb^{3+} and Tm^{3+} was demonstrated, transfer that increases along with Tm^{3+} doping concentration. This study was however limited to low doping concentrations, while in [91] an investigation of the effect of Yb^{3+} codoping on Tm^{3+} ion spectroscopic properties when Yb^{3+} ions content is higher than 2 mol% was conducted with the aim to identify a good candidate active material for short-cavity fiber lasers. This work showed that Yb quenching concentration is of the order of 13 mol% and far larger than Tm quenching concentration, thus allowing to use a Yb:Tm ratio up to 3:1 even for very high Tm concentrations.

The main shortcoming of the widely used TZN tellurite glass as laser material is its low thermal stability, which makes it less durable due to the large amount of heat generated in a laser. To alleviate this problem, a novel Tm^{3+}-doped tungsten tellurite glass composition was developed, with a 50% higher T_g and 36% lower coefficient of thermal expansion (CTE) [92]. The glass was used to demonstrate laser emission in fiber form under excitation through a commercial laser diode operating at 803 nm, although quite a limited slope efficiency (20% with respect to the absorbed pump power) was achieved.

Besides thulium, another RE capable of generating ~2 μm laser emission is holmium (Ho), thanks to the transition $Ho^{3+}: {}^5I_7 \rightarrow {}^5I_8$. Considering the larger emission cross-section and longer lifetime of the lasing state, Ho^{3+} is suitable for ~2 μm laser, particularly for reducing the laser threshold [93]. However, one of the major shortcomings of Ho^{3+} is the lack of ground state absorption transitions that overlap with convenient high-power pump sources, so

codoping with another RE with a strong absorption band at around 800 or 980 nm, such as Yb^{3+} or Tm^{3+}, is commonly used [76, 79, 94].

In [79], 2.0 μm emission characteristics of Ho^{3+} ions both by direct excitation and by sensitized excitation through energy transfer from Yb^{3+} ions in a codoped barium-tellurite glass are detailed. A fluorescence band of 160 nm and an emission cross-section of 1.45×10^{-20} cm^2 were reported. These values resulted to be higher compared to those previously published for other glass systems. The emission intensity of Ho^{3+}: $^5I_7 \rightarrow {}^5I_8$ was measured to be 8 times higher under the excitation at 980 nm through the energy level $^2F_{5/2}$ of Yb^{3+} ion when compared to the direct excitation of Ho^{3+}. This is due to the high absorption cross-section of Yb^{3+} ion alongside the highly efficient (86%) sensitized energy transfer from Yb^{3+}: $^2F_{5/2}$ to Ho^{3+}: $^5I_6$.

Holmium presents also another interesting mid-IR emission at 2.9 μm from the transition Ho^{3+}: $^5I_6 \rightarrow {}^5I_7$. An extensive investigation of this holmium emitting level in a TZGB glass (74.5 TeO_2-12.2 ZnF_2-6.4 GeO_2-4.2 Bi_2O_3) was conducted in [78]. The result indicates that the main issues with this glass are water incorporation and the low luminescence efficiency of $^5I_6$ level (8%). The reported numerical simulations indicated that the prospect for continuous wave (CW) operation on the $^5I_6 \rightarrow {}^5I_7$ transition in Ho^{3+}-doped tellurite glasses is low.

In [95], the 2.9 μm emission from an Yb^{3+}/Ho^{3+}co-doped tellurite glass (80 TeO_2-15 (BaF_2 + BaO)-3 La_2O_3) is investigated. The FWHM of the emission was 180 nm and the peak emission cross-section was 9.1×10^{-21} cm^2, comparable to other hosts and even better than ZBLAN fluoride glass. The emission intensity increased many folds upon Yb^{3+} excitation at 985 nm compared to direct Ho^{3+} ion excitation, thanks to the high absorption of ytterbium at the pump wavelength followed by the resonant energy transfer from Yb^{3+} to Ho^{3+} ions.

Concerning erbium ion, it is an ideal choice for emission in the mid-IR wavelength range, thanks to its fluorescence at 2.7 μm corresponding to the Er^{3+}: $^4I_{11/2} \rightarrow {}^4I_{13/2}$ transition and the possibility to use 808 or 980 nm laser diodes as pumping source.

The potential of erbium-doped tellurite glass for the realization of compact laser devices at this wavelength was extensively investigated in [82]. In this work, it is shown that the presence of OH^- groups in current state-of the-art Er^{3+}-doped tellurite glass is high enough to suppress the 3 μm emission in the glass, due to a large energy transfer from the excited state to the OH^- radical. Moreover, it was calculated from numerical simulations that in the absence of OH^- impurities, the pumping intensity required for population inversion in an Er^{3+}-doped tellurite CW fiber laser pumped at 976 nm is ~80 kW/cm^2 for Er_2O_3 concentrations ≥ 2.65 mol%. It was also established that a pump ESA process at 976 nm would have a detrimental impact on the performance of the fiber laser.

More recently, a barium tellurite glass host was proposed for obtaining 2.7 μm emission from erbium [80]. This glass possesses higher thermal properties compared to typical TZN glass and lower OH^- content, thanks to the addition of BaF_2. An optical fiber was prepared using the developed glass, and 2.7 μm fluorescence was measured upon excitation through a 980 nm laser diode. The feasibility of an Er^{3+}-doped tellurite fiber laser operating at 2.7 μm based on this novel glass was also theoretically investigated, showing that the barium tellurite fiber is a promising candidate for the development of efficient mid-infrared fiber lasers [80].

3. Nonsilica oxide glass optical fiber fabrication

3.1. Optical fibers

The next paragraphs present the very basic concepts of an optical fiber that are relevant to the understanding of the technological challenges behind the manufacturing of multicomponent oxide glass fibers.

A complete description of the concepts and working principles of the optical fibers is out of the scope of this chapter. For a detailed description, the reader can refer to the excellent textbooks given in [96, 97].

The typical configuration of an optical fiber is shown in **Figure 5**. It consists of a core made of a glass with a refractive index value n_{core} surrounded by a cladding glass layer of refractive index $n_{cladding}$. Although this is not always implemented at the academic level, a thin polymer coating (polyamide or acrylate type polymer) should be applied during the drawing process to strengthen mechanically the fiber and to protect it from long-term moisture degradation or other possible chemical contamination sources.

Electromagnetic radiations are confined in the core provided that the refractive index values of the core and cladding glasses meet the condition $n_{core} > n_{cladding}$.

Under this condition, at least one of the so-called electromagnetic or optical modes can be confined and propagate down the optical fiber core. In first approximation, the modes can be understood as a set of constructive interference patterns along the fiber. For illustration purpose, the intensity profile of the electromagnetic fields of few modes is shown in **Figure 6**.

The number of propagating modes depends on the dimension and the difference of refractive index values between the core and the cladding glasses.

The normalized frequency parameter, V, for a step-index optical fiber is given by:

$$V = \frac{2\pi a}{\lambda} \left(n_{core}^2 - n_{clad}^2 \right)^{\frac{1}{2}} \tag{1}$$

where λ is the wavelength in vacuum and a is the radius of the fiber core. If $V < 2.4$, the optical fiber can support only one propagating mode in the core. If any power is launched in the other modes at the fiber input, it will leak into the cladding material.
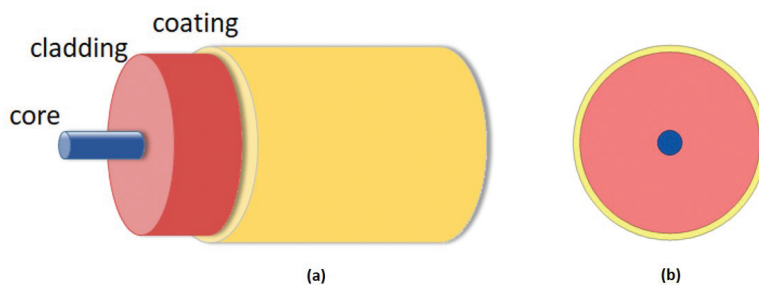

(a)   (b)

Figure 5. (a) Scheme of a typical optical fiber and (b) cross-section illustration of a typical optical fiber structure.
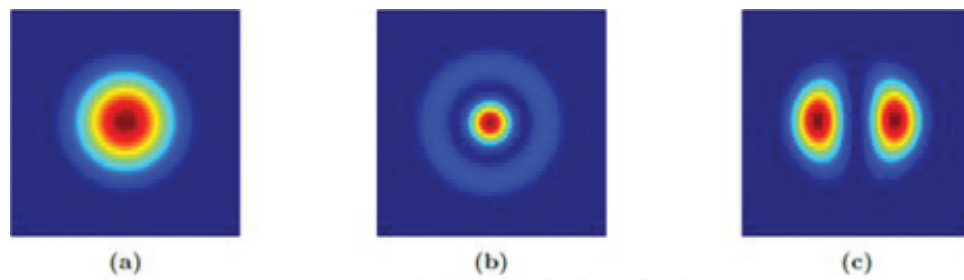
Figure 6. Spatial distribution of the electromagnetic field amplitude of few optical modes in a low numerical aperture multimode fiber: (a) LP_{01} mode or "fundamental mode," (b) LP_{02} mode and (c) LP_{03}.

For numerous applications and in particular for the development of optical coherent sources, single-mode operation is highly desirable. The spatial and temporal properties of the propagating beam in a single-mode fiber can be managed with better control, making this fiber configuration more suitable for the development of high-performance sources.

Typically, a difference value down to 10^{-3} between the refractive index values of the core and the cladding glasses can be achieved. According to equation (1), such refractive index difference value implies that to maintain single-mode operation, a typical core diameter must lay below the values of 15 and 30 μm for wavelengths in the 1 to 2 μm range, respectively

3.2. Double-cladding structure for high-power fiber lasers and amplifiers

The double-cladding strategy was developed to exploit the high pump power available from a laser diode [98]. The structure of the fiber allows to launch high pump power into the first cladding surrounding the core, as reported in **Figure 7**. The pump power is confined within the first cladding, thanks to the second cladding. Along the fiber length, the pump radiation interacts numerous times with the core glass material. At each interaction, the RE ions contained in the core absorb part of the pump power. The excited RE ions subsequently reemit part of the absorbed power by a stimulated emission phenomenon. The reemission being then confined within the core, substantially the double-cladding structure converts low-brightness laser diode power into high-brightness fiber laser.
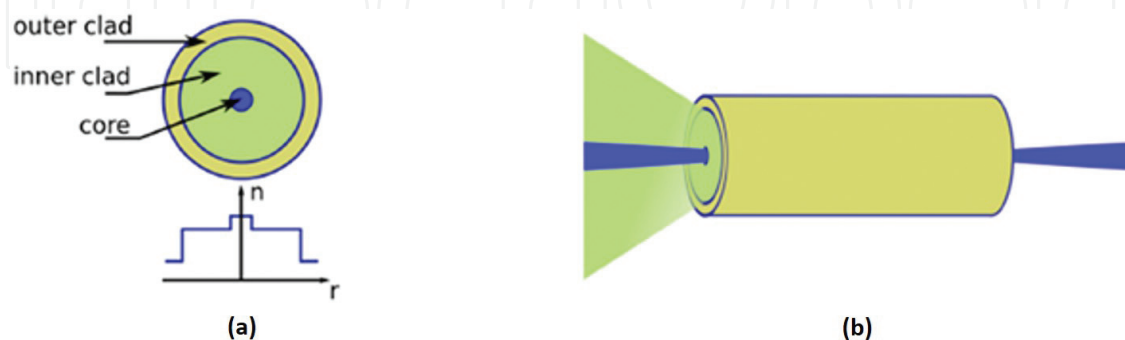

Figure 7. (a) Cross-section image and refractive index profile of a double-cladding fiber for high-power amplifiers and lasers; (b) illustration of the concept of double-cladding structure for a high-power amplifier. Pump laser beam in green, input signal and output amplified signal in blue.

3.3. Preform fiber drawing technique: process and main parameters

The drawing of a soft oxide glass fiber directly from the molten state has been reported [99]; however, the versatility of this approach remains very limited as it requires substantial modification of the drawing facilities in order to change the fiber core/cladding ratio and diameter. Most importantly, the diameter and fiber structural control is difficult to achieve while glass crystallization often occurs at the edges of the crucible walls, impairing both the optical property transmission of the optical fiber due to the presence of scattering crystals and the fiber mechanical robustness.

Actually, as for the advanced silica glass fiber technology, the most employed technique for drawing multicomponent glass fibers is the preform drawing [100]. In this approach, the so-called preform, which is a "macroscopic" version of the fiber, is first manufactured using one of the procedures described in Section 2.1. For multicomponent oxide glass fibers, the typical dimensions of the preform range from 10 to 20 mm in diameter and few cm to 20 cm in length.

The preform is then placed in a drawing tower where it is heated up until the glass reaches a viscosity of about 10^5 Pa s. A schematic illustration of a drawing tower is shown in **Figure 8**. Under the combined effect of gravity and surface tension forces, the softened part of the preform drops down and thins down into a fiber, which is then pulled either using a capstan or attached directly onto a rotating drum at the bottom of the tower. The control of the dimension at the mm scale of the preform and the relatively high tensions, typically 0.1–1 N, of the drawing process allows for a very precise control of the final fiber dimensions and geometry.

The control of the fiber diameter is achieved by tuning the speed at which the preform is being fed into the furnace and the speed at which the fiber is being drawn from the preform. For an

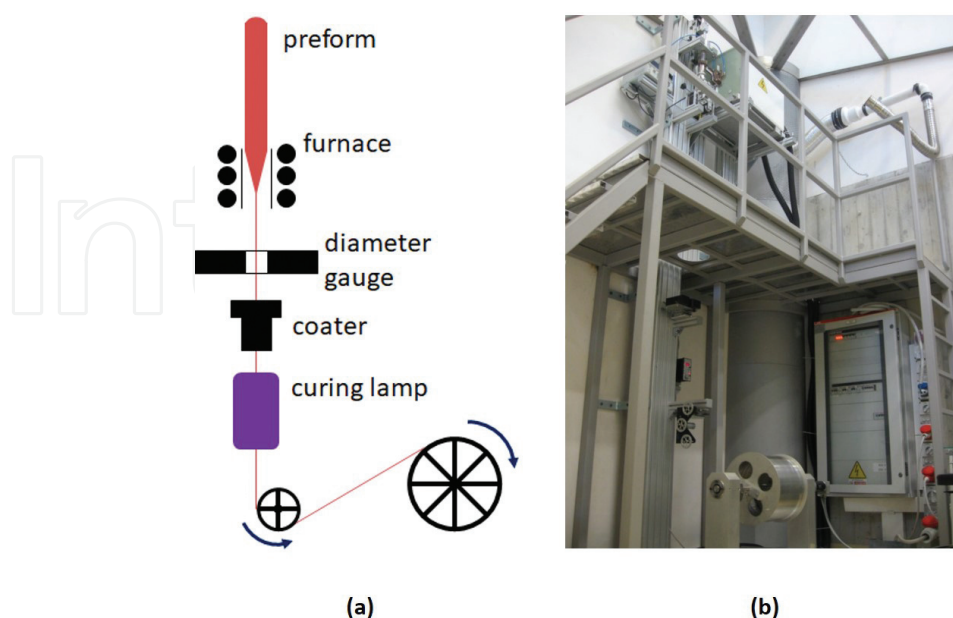(a)   (b)

Figure 8. (a) Schematic illustration of a fiber drawing tower, which implements the preform drawing approach; (b) photography of an in-house developed drawing tower installed at Politecnico di Torino.

incompressible liquid, mass conservation considerations lead to the following equation for the fiber diameter d_{fiber}:

$$d_{fiber} = d_{preform} \left(\frac{v_{preform}}{v_{fiber}} \right)^{\frac{1}{2}}$$
(2)

where $d_{preform}$ is the preform diameter and $v_{preform}$ and v_{fiber} are, respectively, the preform feed speed and the pulling speed.

3.3.1. Drawing tower facilities

Commercial towers for soft glasses can be acquired from several specialized manufacturers; however, a cost-effective drawing tower can be developed in-house and leads to similar results in terms of fiber diameter fluctuations, which are typically of ± 1 µm over few tens of meters of fiber. For multicomponent oxide glasses, the main source of fluctuations/contaminations in the final fiber arises at the production stage of the preform, not during the drawing process itself.

The fiber drawing process of a multicomponent glass preform is carried out at a typical speed ranging from few m/min to 30 m/min at most. This is in contrast to the very high drawing speed used to produce telecom silica glass optical fiber, which reaches up to 20 m/s [100]. Because of this slow drawing speed, automated diameter adjustment through a diameter monitor feedback can be rather inefficient, especially in the academic field where very often one fiber is different from the next in terms of its glass composition or structure. As such, the furnace configuration and the feeding procedure of the preform into the furnace become crucial to ensure the diameter stability during the drawing process. Beside obvious parameters such as the temperature stability of the furnace, ensuring a steady laminar flow around the preform during the drawing procedure is key. The choice of the gas used N_2/O_2, Ar or N_2 depends strongly on the glass composition. The low gas content in H_2O is however necessary to avoid any detrimental effects, optical or mechanical, on the drawn fiber.

The furnace can be based on either resistive elements or an induction head where the susceptor consists of a simple metal or graphite ring. The latter approach offers the possibility to tailor easily and cost-effectively the hot zone by simply changing the susceptors.

3.4. Preform fabrication

3.4.1. Rod-in-tube

In the rod-in-tube technique, the preform consists, in its most simple form, of a rod of core glass inserted into a cladding glass tube. When heated up inside the drawing tower furnace, the cladding tube collapses around the core rod under the effect of gravity and surface tension forces. The two glass materials are then drawn together as a single concentrically structured fiber. For the process to take place in a controlled manner and to avoid excessive residual stress within the fiber, several important material aspects need to be taken into consideration. The two glasses must match in terms of thermomechanical properties: glass working temperature, glass transition temperature and thermal expansion values of the two glasses should match as

much as possible. In practice, these constrains imply that the two glasses have similar compositions, which in turn limit the upper range of the refractive index difference value achievable.

It is also preferable that both the tube inner diameter and the rod diameter match each other closely to avoid structural deformation of the core or trapped air at the interface between the two glasses. The latter issue can be addressed by applying vacuum on the top part of the preform.

As illustrated in **Figure 9**, to achieve a small diameter core dimension or manufacture the double-cladding structure, the preform preparation consists in an intermediate step where a core/cladding preform is thinned down into a cane, which is then inserted into another cladding tube to form a new preform. This process can be repeated several times depending on the thermal stability against crystallization of the glass compositions involved. This cane drawing process is carried out in the drawing tower but at higher viscosity and under higher tension than the fiber drawing process.

3.4.2. Core glass rod manufacture

The core glass rod arises from a single bulk glass casted into either a cylindrical- or rectangular-shaped mold. In the latter case, the bulk can then be machined into a cylindrical rod of the desired dimension. In both cases, the core glass rod needs to be polished preferably using a nonaqueous cooling liquid so as not to impair the optical transmission of the fiber.
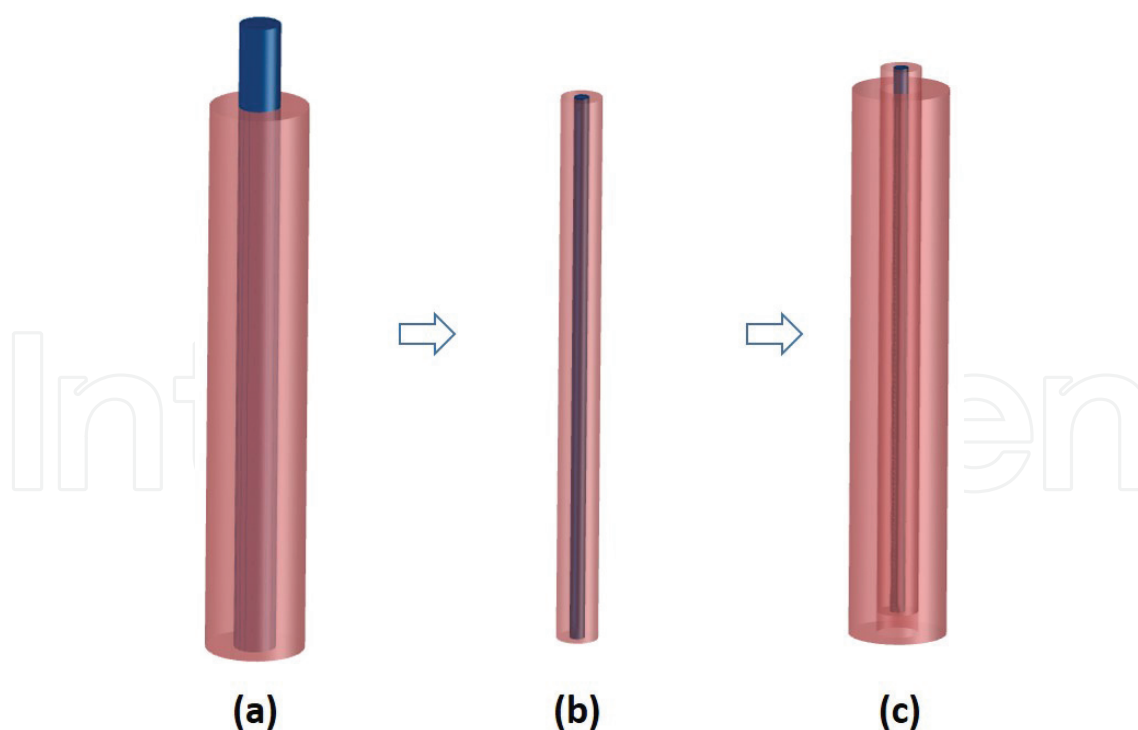

(a)   (b)   (c)

Figure 9. (a) Implementation of an optical fiber preform using the rod-in-tube technique. Core glass rod in blue, cladding glass tube in red; (b) glass cane with a core/cladding structure obtained by drawing the preform shown in (a); (c) implementation of a small core/cladding diameter ratio preform by inserting the rod shown in (b) into an additional cladding glass tube.

3.4.3. Cladding glass tube

3.4.3.1. Drilling

The cladding tube can be manufactured through different techniques. Drilling is carried out either using an ultrasonic drilling setup and/or using specialized diamond drilling bits. This approach allows for machining tubes reliably and with a great precision, making possible a precise control of the fiber dimensions through the drawing process. In addition, the glass does not go through a heating cycle, which could favor crystallization tendency.

There are, however, a number of drawbacks. Because of the brittleness of the glass, this is a slow and therefore time-consuming process. Drilling small diameter holes cannot be achieved over long lengths due to the mechanical flexibility of the drill bit itself. Thin wall tubes are also difficult to manufacture. Adding to the processing time, following drilling, the tube must undergo an additional polishing process not only to smoothen the wall roughness but also to clean up the walls from free glass particles that can be prone to crystallization during the drawing process.

3.4.3.2. Extrusion

An overview of the overall procedure and equipment of the extrusion process is given in [101–102]. In the extrusion process, a bulk glass, typically 30 mm in diameter and 30–50 mm high, is loaded into a furnace apparatus open on top and bottom. A scheme of the process is reported in **Figure 10**. The glass is heated up to a temperature corresponding to a viscosity of 10^8 Pa s. On the top part, a press ram applies a force on the glass bulk. The soften glass exits through the
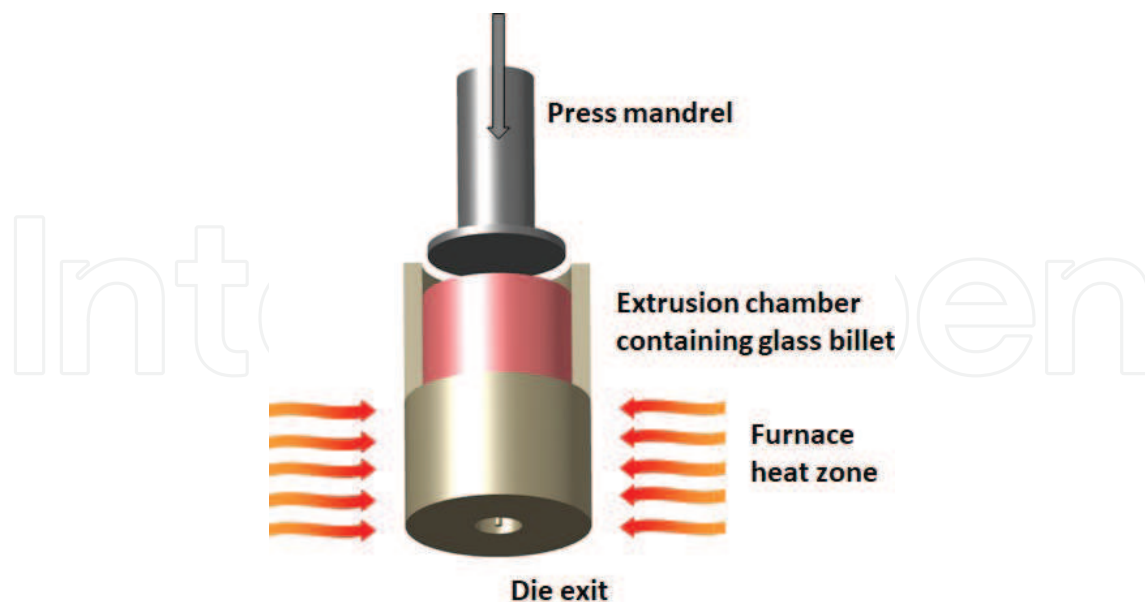

Figure 10. Schematic of the extrusion process for manufacturing glass tubes. A glass billet (in red) is heated up until the glass reaches a viscosity of typically 10^8 Pa s. A high pressure is then applied onto the top billet surface through a mandrel. The softened glass is then slowly pushed out of the die through the bottom orifice of this latter. The orifice arrangement with a pin in its center allows for producing a glass tube.

bottom part of the apparatus, which consists of a funnel shape die where a spider setup allows for a pin to be held in the center of the die.

Typically, the pressure applied ranges from 1 to 6 GPa. For multicomponent oxide glasses, the dies can be manufactured out of standard stainless-steel material, although less reactive (more stable and inert) metals such as Inconel are sometimes preferable depending on the temperatures and glass compositions involved. The die surface finish plays an important role onto the surface quality finish of the extruded glass tube itself. Indeed, it is possible to extrude very high-quality surface finish tubes also because the process is carried out at a range of viscosity where surface tension is still effective.

Some swelling effect can occur and tends to distort the preform and modify its dimensions with respect to the die dimension. However, this effect can be limited through pertinent die design and temperature of operation. If compared to the drilling technique, the main disadvantage of the extrusion is that the glass goes through an extra heating cycle above the glass transition temperature (T_g), which can promote glass nucleation and crystallization. Nevertheless, the negative effect of this cycle is limited by the fact that the viscosity range considered is substantially high.

3.4.3.3. Rotational casting

The rotational casting [103] is carried out by casting the molten glass into a cylindrical mold (**Figure 11**), which is then tilted horizontally and rotated at a rotation speed ranging typically from 1000 to 2000 rpm while the glass inside the mold is still liquid. As the liquid cools down, it forms a glass tube inside the mold, which is then loaded into a furnace for glass annealing. Despite being a "manual craft" operation, if processed under the same conditions, the tube
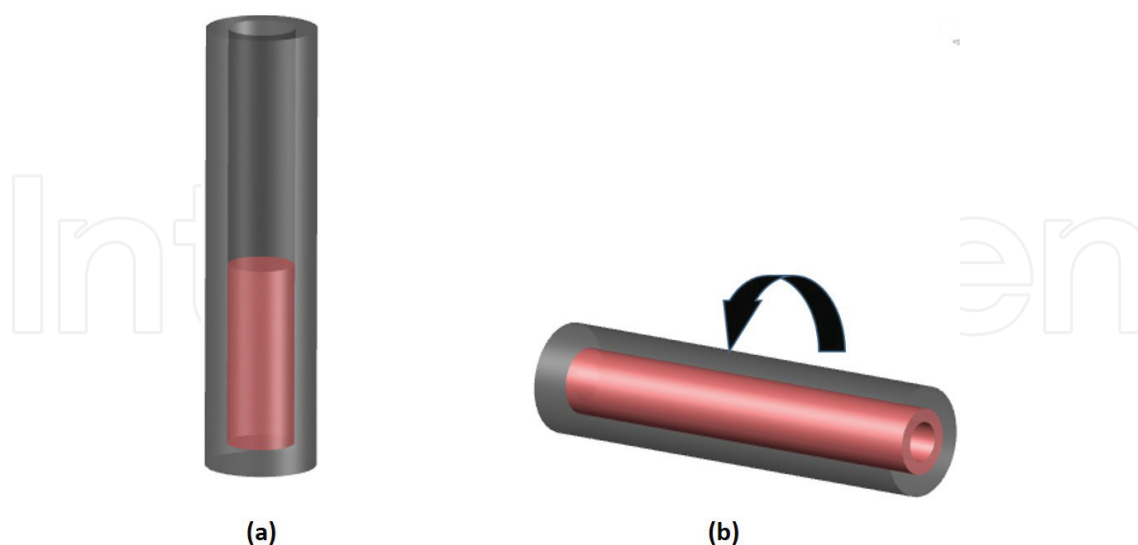

(a)   **(b)**

Figure 11. Schematic of the rotational casting procedure for manufacturing glass tubes: (a) the molten glass is cast into a mold held in vertical position; (b) the mold is tilted in the horizontal direction and then rotated at high speed. A glass tube forms along the mold internal walls.

inner diameter value is commonly reproducible within $\pm 5\%$. The typical roughness value of the inner tube surface is below 10 nm. Such pristine surface is indeed particularly suitable for the development of optical fibers.

The rotational casting process takes place in a matter of seconds, making it a very fast production technique if compared to the two approaches described above. The main limitation of the rotational casting technique regards the range of inner tube diameter values achievable. Uniform tubes with small or large inner diameters can be difficult to achieve in a reproducible manner. Also, the technique is foremost restricted to glass compositions that display a low viscosity once molten. Silicate glasses, for instance, are unpractical for implementing the rotational casting technique.

3.4.4. Built-in-casting and suction casting approaches

The built-in-casting and suction casting techniques [104, 105] were developed to avoid some of the issues inherent to the rod-in-tube technique, the main purpose being to manufacture a single unit core/cladding structured preform. Both techniques involve the casting of the core material in a liquid state inside a cladding tube for the former approach or on the top of the cooling cladding glass for the latter approach.

These techniques can provide substantially low loss optical fibers and display the advantage to require low processing time. However, the control on the dimension and shape of the core is rather limited with, therefore, a very low reproducibility. Some degree of diffusion process also occurs at the interface between the two glasses. Because of these features, these techniques are being used only at an academic level.

Author details

Daniel Milanese[1,6]*, Joris Lousteau[2], Xiushan Zhu[3], Arturo Chavez-Pirson[4], Diego Pugliese[1], Nadia Giovanna Boetti[5] and Nasser Peyghambarian[3,4]

*Address all correspondence to: daniel.milanese@polito.it

1 Department of Applied Science and Technology and RU INSTM, Politecnico di Torino, Torino, Italy

2 Optoelectronics Research Centre, University of Southampton, Southampton, United Kingdom

3 College of Optical Sciences, University of Arizona, Tucson, AZ, United States of America

4 NP Photonics Inc., Tucson, AZ, United States of America

5 Istituto Superiore Mario Boella, Torino, Italy

6 Consiglio Nazionale delle Ricerche, Istituto di Fotonica e Nanotecnologie, Trento, Italy

References

[1] Rasmussen SC. How Glass Changed the World: The History and Chemistry of Glass from Antiquity to the 13th Century. 1st ed. Berlin: Springer; 2012. 85 p. DOI: 10.1007/978-3-642-28183-9

[2] Varshneya AK. Fundamentals of Inorganic Glasses. 1st ed. New York, USA: Academic Press Inc.; 1994. 570 p

[3] Yamane M, Asahara Y. Glasses for Photonics. 1st ed. Cambridge, UK: Cambridge University Press; 2004. 282 p.

[4] Digonnet MJF, editor. Rare-Earth-Doped Fiber Lasers and Amplifiers. 1st ed. Boca Raton, FL, USA: CRC Press; 2001. 798 p

[5] Brawer SA, White WB. Raman spectroscopic investigation of the structure of silicate glasses. I. The binary alkali silicates. The Journal of Chemical Physics. 1975;**63**:2421-2432. DOI: 10.1063/1.431671

[6] Quimby RS, Miniscalco WJ, Thompson B. Clustering in erbium-doped silica glass fibers analyzed using 980 nm excited-state absorption. Journal of Applied Physics. 1994;**76**:4472-4478. DOI: 10.1063/1.357278

[7] Kitamura R, Pilon L, Jonasz M. Optical constants of silica glass from extreme ultraviolet to far infrared at near room temperature. Applied Optics. 2007;**46**:8118-8133. DOI: 10.1364/AO.46.008118

[8] France PW, editor. Fluoride Glass Optical Fibers. 1st ed. Glasgow and London: Blackie and Sons Ltd; 1990. 280 p.

[9] Seddon AB. Chalcogenide glasses: A review of their preparation, properties and applications. Journal of Non-Crystalline Solids. 1995;**184**:44-50. DOI: 10.1016/0022-3093(94)00686-5

[10] Falconi MC, Palma G, Starecki F, Nazabal V, Troles J, Taccheo S, Ferrari M, Prudenzano F. Design of an efficient pumping scheme for mid-IR Dy^{3+}:$Ga_5Ge_{20}Sb_{10}S_{65}$ PCF fiber laser. IEEE Photonics Technology Letters. 2016;**28**:1984-1987. DOI: 10.1109/LPT.2016.2581022

[11] Jackson SD, Lancaster DG. Fiber lasers that bridge the shortwave to midwave regions of the infrared spectrum. In: Okhotnikov OG, editor. Fiber Lasers. 1st ed. Weinheim: Wiley-VCH; 2012. pp. 233-267. DOI: 10.1002/9783527648641.ch7

[12] Wang JS, Vogel EM, Snitzer E. Tellurite glass: A new candidate for fiber devices. Optical Materials. 1994;**3**:187-203. DOI: 10.1016/0925-3467(94)90004-3

[13] Yiannopoulos YD, Varsamis CPE, Kamitsos EI. Density of alkali germanate glasses related to structure. Journal of Non-Crystalline Solids. 2001;**293–295**:244-249. DOI: 10.1016/S0022-3093(01)00677-9

[14] Veeranna Gowda VC. Physical, thermal, infrared and optical properties of Nd^{3+} doped lithium-lead-germanate glasses. Physica B: Condensed Matter. 2015;**456**:298-305. DOI: 10.1016/j.physb.2014.09.004

[15] Sidek HAA, Bahari HR, Halimah MK, Yunus WMM. Preparation and elastic moduli of germanate glass containing lead and bismuth. International Journal of Molecular Sciences. 2012;**13**:4632-4641. DOI: 10.3390/ijms13044632

[16] Polyanskiy MN. Refractive Index Database [Internet]. 2017. Available from: https://refractiveindex.info/ [Accessed: 2017–11-18]

[17] Jiang X, Lousteau L, Richards B, Jha A. Investigation on germanium oxide-based glasses for infrared optical fibre development. Optical Materials. 2009;**31**:1701-1706. DOI: 10.1016/j.optmat.2009.04.011

[18] Munasinghe HT, Winterstein-Beckmann A, Schiele C, Manzani D, Wondraczek L, Afshar VS, Monro TM, Ebendorff-Heidepriem H. Lead-germanate glasses and fibers: A practical alternative to tellurite for nonlinear fiber applications. Optical Materials Express. 2013;**3**:1488-1503. DOI: 10.1364/OME.3.001488

[19] Rawson H. Properties and Applications of Glass. 1st ed. Amsterdam: Elsevier Science Ltd; 1980. 318 p.

[20] Vogel W. Glass Chemistry. 1st ed. Berlin: Springer Verlag; 1994. 478 p. DOI: 10.1007/978-3-642-78723-2

[21] Baikova LG, Pukh VP, Fedorov YK, Sinani AB, Tikhonova LV, Kireenko MF. Mechanical properties of phosphate glasses as a function of the total bonding energy per unit volume of glass. Glass Physics and Chemistry. 2008;**34**:126-131. DOI: 10.1134/S1087659608020028

[22] Karabulut M, Melnik E, Stefan R, Marasinghe GK, Ray CS, Kurkjian CR, Day DE. Mechanical and structural properties of phosphate glasses. Journal of Non-Crystalline Solids. 2001;**288**:8-17. DOI: 10.1016/S0022-3093(01)00615-9

[23] Fuchs RJ. Method of softening hard water with sodium phosphate glasses. US Patent No. US 3130152 A; 1964

[24] Ahmed I, Lewis M, Olsen I, Knowles JC. Phosphate glasses for tissue engineering: Part 1. Processing and characterisation of a ternary-based P_2O_5-CaO-Na_2O glass system. Biomaterials. 2004;**25**:491-499. DOI: 10.1016/S0142-9612(03)00546-5

[25] Sales BC, Boatner LA. Lead-iron phosphate glass: A stable storage medium for high-level nuclear waste. Science. 1984;**226**:45-48. DOI: 10.1126/science.226.4670.45

[26] Kreidl NJ, Weyl WA. Phosphates in ceramic ware: IV, phosphate glasses. Journal of the American Ceramic Society. 1941;**24**:372-378. DOI: 10.1111/j.1151-2916.1941.tb15444.x

[27] Campbell JH, Hayden JS, Marker A. High-power solid-state lasers: A laser glass perspective. International Journal of Applied Glass Science. 2011;**2**:3-29. DOI: 10.1111/j.2041-1294.2011.00044.x

[28] Brow RK. Review: The structure of simple phosphate glasses. Journal of Non-Crystalline Solids. 2000;**263-264**:1-28. DOI: 10.1016/S0022-3093(99)00620-1

[29] Myers JD, Vollers CS. Laser phosphate glass compositions. US Patent No. US 4248732 A; 1978

[30] Hayden J. Phosphate glass useful in lasers. US Patent No. US 5334559 A; 1994

[31] Brow RK, Click CA, Alam TM. Modifier coordination and phosphate glass networks. Journal of Non-Crystalline Solids. 2000;**274**:9-16. DOI: 10.1016/S0022-3093(00)00178-2

[32] Seneschal K, Smektala F, Bureau B, Le Floch M, Jiang S, Luo T, Lucas J, Peyghambarian N. Properties and structure of high erbium doped phosphate glass for short optical fibers amplifiers. Materials Research Bulletin. 2005;**40**:1433-1442. DOI: 10.1016/j.materresbull.2005.05.004

[33] Harada T, In H, Takebe H, Morinaga K. Effect of B_2O_3 addition on the thermal stability of barium phosphate glasses for optical fiber devices. Journal of the American Ceramic Society. 2004;**87**:408-411. DOI: 10.1111/j.1551-2916.2004.00408.x

[34] Brow RK. Nature of alumina in phosphate glass: I, properties of sodium aluminophosphate glass. Journal of the American Ceramic Society. 1993;**76**:913-918. DOI: 10.1111/j.1151-2916.1993.tb05315.x

[35] Bingham PA, Hand RJ, Hannant OM, Forder SD, Kilcoyne SH. Effects of modifier additions on the thermal properties, chemical durability, oxidation state and structure of iron phosphate glasses. Journal of Non-Crystalline Solids. 2009;**355**:1526-1538. DOI: 10.1016/j.jnoncrysol.2009.03.008

[36] Martin WE, Milam D. Gain saturation in Nd:doped laser materials. IEEE Journal of Quantum Electronics. 1982;**18**:1155-1163. DOI: 10.1109/JQE.1982.1071668

[37] Campbell JH, Wallerstein EP, Hayden JS, Sapak D, Marker AJ. Effects of melting conditions on platinum-inclusion content in phosphate laser glasses. Glass Science and Technology. 1995;**68**:11-21. DOI: 10.4135/9781483327211.n2

[38] Karlsson G, Laurell F, Tellefsen J, Denker B, Galagan B, Osiko V, Sverchkov S. Development and characterization of Yb-Er laser glass for high average power laser diode pumping. Applied Physics B: Lasers and Optics. 2002;**75**:41-46. DOI: 10.1007/s00340-002-0950-4

[39] Lee YW, Sinha S, Digonnet MJF, Byer RL. 20 W single-mode Yb^{3+}-doped phosphate fiber laser. Optics Letters. 2006;**31**:3255-3257. DOI: 10.1364/OL.31.003255

[40] Polynkin A, Polynkin P, Schülzgen A, Mansuripur M, Peyghambarian N. Watts-level, short all-fiber laser at 1.5 μm with a large core and diffraction-limited output via intracavity spatial-mode filtering. Optics Letters. 2005;**30**:403-405. DOI: 10.1364/OL.30.000403

[41] Gapontsev VP, Matitsin SM, Isineev AA, Kravchenko VB. Erbium glass lasers and their applications. Optics and Laser Technology. 1982;**14**:189-196. DOI: 10.1016/0030-3992(82)90095-0

[42] Fermann ME, Hanna DC, Shepherd DP, Suni PJ, Townsend JE. Efficient operation of an Yb-sensitized Er fibre laser at 1.56 μm. Electronics Letters. 1988;**24**:1135-1136. DOI: 10.1049/el:19880772

[43] Barnes WL, Poole SB, Townsend JE, Reekie L, Taylor DJ, Payne DN. Er^{3+}/Yb^{3+} and Er^{3+} doped fiber lasers. Journal of Lightwave Technology. 1989;**7**:1461-1465. DOI: 10.1109/50.39081

[44] Hwang B-C, Jiang S, Luo T, Watson J, Sorbello G, Peyghambarian N. Cooperative upconversion and energy transfer of new high Er^{3+}- and Yb^{3+}–Er^{3+}-doped phosphate glasses. Journal of the Optical Society of America B: Optical Physics. 2000;**17**:833-839. DOI: 10.1364/JOSAB.17.000833

[45] Wu R, Myers JD, Myers MJ, Rapp C. Fluorescence lifetime and 980nm pump energy transfer dynamics in erbium and ytterbium co-doped phosphate laser glasses. In: Proceedings of SPIE 4968, Solid State Lasers XII; 28–30 January 2003; San Jose. Bellingham, WA, USA: SPIE; 2003. pp. 11-17

[46] Margaryan A, Piliavin MA. Germanate Glasses: Structure, Spectroscopy and Properties. 1st ed. Artech House: Boston and London; 1993. 200 p

[47] Sakaguchi S, Todoroki S. Optical properties of GeO_2 glass and optical fibers. Applied Optics. 1997;**36**:6809-6814. DOI: 10.1364/AO.36.006809

[48] Higby PL, Aggarwal ID. Properties of barium gallium germanate glasses. Journal of Non-Crystalline Solids. 1993;**163**:303-308. DOI: 10.1016/0022-3093(93)91308-P

[49] Lezal D, Pedlíková J, Horák J. GeO_2–PbO glassy system for infrared fibers for delivery of Er:YAG laser energy. Journal of Non-Crystalline Solids. 1996;**196**:178-182. DOI: 10.1016/0022-3093(95)00582-X

[50] Cherukuri SC, Pye LD. Faraday rotation of rare earth alkali germanate glasses. In: McCarthy GJ, Silber HB, Rhyne JJ, Kalina FM, editors. The Rare Earths in Modern Science and Technology. 1st ed. Berlin: Springer; 1982. pp. 465-469. DOI: 10.1007/978-1-4613-3406-4_99

[51] Evstropiev KS, Ivanov AO. Physikalisch-chemische eigenschaften von germaniumgläsern. In: Matson FR, Rindone GE, editors. Advances in Glass Technology, Part 2. 1st ed. New York: Plenum Press; 1963. pp. 79-85

[52] Henderson GS. The germanate anomaly: What do we know? Journal of Non-Crystalline Solids. 2007;**353**:1695-1704. DOI: 10.1016/j.jnoncrysol.2007.02.037

[53] Wang J, Lincoln JR, Brocklesby WS, Deol RS, Mackechnie CJ, Pearson A, Tropper AC, Hanna DC, Payne DN. Fabrication and optical properties of lead-germanate glasses and a new class of optical fibers doped with Tm^{3+}. Journal of Applied Physics. 1993;**73**:8066-8075. DOI: 10.1063/1.353922

[54] Xu R, Xu L, Hu L, Zhang J. Structural origin and laser performance of thulium-doped germanate glasses. The Journal of Physical Chemistry. A. 2011;**115**:14163-14167. DOI: 10.1021/jp207574m

[55] Braud A, Girard S, Doualan JL, Thuau M, Moncorgé R. Energy-transfer processes inYb:Tm-doped KY_3F_{10}, $LiYF_4$, and BaY_2F_8 single crystals for laser operation at 1.5 and 2.3 μm. Physical Review B. 2000;**61**:5280-5292. DOI: 10.1103/PhysRevB.61.5280

[56] Fang Y, Zhao G, Xu J, Zhang N, Ma Z, Hu L. Energy transfer and 1.8 μm emission in Yb^{3+}/Tm^{3+} co-doped bismuth germanate glass. Ceramics International. 2014;**40**:6037-6043. DOI: 10.1016/j.ceramint.2013.11.053

[57] Richards B, Shen S, Jha A, Tsang Y, Binks D. Infrared emission and energy transfer in Tm^{3+}, Tm^{3+}-Ho^{3+} and Tm^{3+}-Yb^{3+}-doped tellurite fibre. Optics Express. 2017;**15**:6546-6551. DOI: 10.1364/OE.15.006546

[58] Wang WC, Yuan J, Chen DD, Zhang JJ, Xu SQ, Zhang QY. Enhanced 1.8 μm emission in Cr^{3+}/Tm^{3+} co-doped fluorogermanate glasses for a multi-wavelength pumped near-infrared lasers. AIP Advances. 2014;**4**:107145. DOI: 10.1063/1.4900860

[59] Subramanyam Y, Moorthy LR, Lakshman SVJ. Determination of radiative transitions of Ho^{3+} in various ternary sulphate glasses from absorption measurements. Physics and Chemistry of Glasses. 1992;**33**:21-23

[60] Xu R, Pan J, Hu L, Zhang J. 2.0 μm emission properties and energy transfer processes of Yb^{3+}/Ho^{3+} codoped germanate glass. Journal of Applied Physics. 2010;**108**:043522. DOI: 10.1063/1.3468726

[61] Cai M, Zhou B, Tian Y, Zhou J, Xu S, Zhang J. Broadband mid-infrared 2.8 μm emission in Ho^{3+}/Yb^{3+}-codoped germanate glasses. Journal of Luminescence. 2016;**171**:143-148. DOI: 10.1016/j.jlumin.2015.11.016

[62] Xu R, Wang M, Tian Y, Hu L, Zhang J. 2.05 μm emission properties and energy transfer mechanism of germanate glass doped with Ho^{3+}, Tm^{3+}, and Er^{3+}. Journal of Applied Physics. 2011;**109**:053503. DOI: 10.1063/1.3553877

[63] Cai M, Wei T, Zhou B, Tian Y, Zhou J, Xu S, Zhang J. Analysis of energy transfer process based emission spectra of erbium doped germanate glasses for mid-infrared laser materials. Journal of Alloys and Compounds. 2015;**626**:165-172. DOI: 10.1016/j.jallcom.2014.11.077

[64] Cai M, Zhou B, Wang F, Wei T, Tian Y, Zhou J, Xu S, Zhang J. R_2O_3 (R = La, Y) modified erbium activated germanate glasses for mid-infrared 2.7 μm laser materials. Scientific Reports. 2015;**5**:13056. DOI: 10.1038/srep13056

[65] El-Mallawany R. Tellurite glasses. Part 1. Elastic properties. Materials Chemistry and Physics. 1998;**53**:93-120. DOI: 10.1016/S0254-0584(97)02041-5

[66] Naftaly M, Shen S, Jha A. Tm^{3+}-doped tellurite glass for a broadband amplifier at 1.47 μm. Applied Optics. 2000;**39**:4979-4984. DOI: 10.1364/AO.39.004979

[67] Wang G, Jiang T, Li C, Yang H, Wang A, Zhang Z. Octave-spanning spectrum of femtosecond Yb:fiber ring laser at 528 MHz repetition rate in microstructured tellurite fiber. Optics Express. 2013;**21**:4703-4708. DOI: 10.1364/OE.21.004703

[68] Shiyu Y, Lousteau J, Olivero M, Merlo M, Boetti N, Abrate S, Chen Q, Chen Q, Milanese D. Analysis of Faraday effect in multimode tellurite glass optical fiber for magneto-optical sensing and monitoring applications. Applied Optics. 2012;**51**:4542-4546. DOI: 10.1364/AO.51.004542

[69] Sakida S, Hayakawa S, Yoko T. Part 2. [125]Te NMR study of M_2O-TeO_2 (M = Li, Na, K, Rb and Cs) glasses. Journal of Non-Crystalline Solids. 1999;**243**:13-25. DOI: 10.1016/S0022-3093(98)00812-6

[70] Himei Y, Miura Y, Nanba T, Osaka A. X-ray photoelectron spectroscopy of alkali tellurite glasses. Journal of Non-Crystalline Solids. 1997;**211**:64-71. DOI: 10.1016/S0022-3093(96)00628-X

[71] Suehara S, Hishita S, Inoue S, Nukui A. Cluster calculational approach to tellurite glasses. Physical Review B. 1998;**58**:14124-14126. DOI: 10.1103/PhysRevB.58.14124

[72] McLaughlin JC, Tagg SL, Zwanziger JW, Haeffner DR, Shastri SD. The structure of tellurite glass: A combined NMR, neutron diffraction, and X-ray diffraction study. Journal of Non-Crystalline Solids. 2000;**274**:1-8. DOI: 10.1016/S0022-3093(00)00199-X

[73] Michel JC, Morin D, Auzel F. Propriétés spectroscopiques et effet laser d'un verre tellurite et d'un verre phosphate fortement dopés en néodyme. Rev. Phys. Appl. 1978; **13**:859-866. DOI: 10.1051/rphysap:019780013012085900

[74] Reisfeld R, Jørgensen CK. Excited state phenomena in vitreous materials. In: Gschneidner KA, Eyring L, editors. Handbook on the Physics and Chemistry of Rare Earths. 1st ed. Amsterdam: Elsevier; 1987. pp. 1-90

[75] Jackson SD. Towards high-power mid-infrared emission from a fibre laser. Nature Photonics. 2012;**6**:423-431. DOI: 10.1038/nphoton.2012.149

[76] Richards B, Jha A, Tsang Y, Binks D, Lousteau J, Fusari F, Lagatsky A, Brown C, Sibbett W. Tellurite glass lasers operating close to 2 μm. Laser Physics Letters. 2010;**7**:177-193. DOI: 10.1002/lapl.200910131

[77] Gomes L, Lousteau J, Milanese D, Scarpignato GC, Jackson SD. Energy transfer and energy level decay processes in Tm^{3+}-doped tellurite glass. Journal of Applied Physics. 2012;**111**:063105. DOI: 10.1063/1.3694747

[78] Gomes L, Milanese D, Lousteau J, Boetti N, Jackson SD. Energy level decay processes in Ho^{3+}-doped tellurite glass relevant to the 3 μm transition. Journal of Applied Physics. 2011;**109**:103110. DOI: 10.1063/1.3587476

[79] Balaji S, Sontakke AD, Sen R, Kalyandurg A. Efficient ~2.0 μm emission from Ho^{3+} doped tellurite glass sensitized by Yb^{3+} ions: Judd-Ofelt analysis and energy transfer mechanism. Optical Materials Express. 2011;**1**:138-150. DOI: 10.1364/OME.1.000138

[80] Wang WC, Yuan J, Li LX, Chen DD, Qian Q, Zhang QY. Broadband 2.7 μm amplifed spontaneous emission of Er^{3+} doped tellurite fibers for mid-infrared laser applications. Optical Materials Express. 2015;**5**:2964-2977. DOI: 10.1364/OME.5.002964

[81] Tian Y, Li B, Chen R, Xia J, Jing X, Zhang J, Xu S. Thermal stability and 2.7 μm spectroscopic properties in Er^{3+} doped tellurite glasses. Solid State Sciences. 2016;**60**:17-22. DOI: 10.1016/j.solidstatesciences.2016.07.012

[82] Gomes L, Oermann M, Ebendorff-Heidepriem H, Ottaway D, Monro T, Librantz AFH, Jackson SD. Energy level decay and excited state absorption processes in erbium-doped tellurite glass. Journal of Applied Physics. 2011;**110**:083111. DOI: 10.1063/1.3651399

[83] Pollnau M, Jackson SD. Mid-infrared fiber lasers. In: Sorokina IT, Vodopyanov KL, editors. Solid-State Mid-Infrared Laser Sources. 1st ed. Berlin Heidelberg: Springer-Verlag; 2003. pp. 225-261. DOI: 10.1007/3-540-36491-9

[84] Richards B, Tsang Y, Binks D, Lousteau J, Jha A. Efficient ~2 μm Tm^{3+}-doped tellurite fiber laser. Optics Letters. 2008;**33**:402-404. DOI: 10.1364/OL.33.000402

[85] Gebavi H, Milanese D, Balda R, Chaussedent S, Ferrari M, Fernandez J, Ferraris M. Spectroscopy and optical characterization of thulium doped TZN glasses. Journal of Physics D: Applied Physics. 2010;**43**:135104. DOI: 10.1088/0022-3727/43/13/135104

[86] Percival RM, Szebesta D, Davey ST. Thulium doped terbium sensitised CW fluoride fibre laser operating on the 1.47 μm transition. Electronics Letters. 1993;**29**:1054-1056. DOI: 10.1049/el:19930703

[87] Miniscalco WJ. Optical and electronic properties of rare earth ions in glasses. In: Digonnet MJF, editor. Rare Earth Doped Fiber Lasers and Amplifiers. 2nd ed. New York: Marcel Dekker; 2001. pp. 17-112. DOI: 10.1201/9780203904657

[88] Jackson SD, King TA. Theoretical modeling of tm-doped silica fiber lasers. Journal of Lightwave Technology. 1999;**17**:948-956. DOI: 10.1109/50.762916

[89] Huang L, Shen S, Jha A. Near infrared spectroscopic investigation of Tm^{3+}–Yb^{3+} co-doped tellurite glasses. Journal of Non-Crystalline Solids. 2004;**345-346**:349-353. DOI: 10.1016/j.jnoncrysol.2004.08.042

[90] Richards B, Tsang Y, Binks D, Lousteau J, Jha A. ~2 μm Tm^{3+}/Yb^{3+}-doped tellurite fibre laser. Journal of Materials Science: Materials in Electronics. 2009;**20**:S317-S320. DOI: 10.1007/s10854-008-9598-0

[91] Milanese D, Gebavi H, Lousteau J, Ferraris M, Schülzgen A, Li L, Peyghambarian N, Taccheo S, Auzel F. Tm^{3+} and Yb^{3+} co-doped tellurite glasses for short cavity optical fiber lasers: Fabrication and optical characterization. Journal of Non-Crystalline Solids. 2010; **356**:2378-2383. DOI: 10.1016/j.jnoncrysol.2010.03.029

[92] Li K, Zhang G, Hu L. Watt-level ~2 μm laser output in Tm^{3+}- doped tungsten tellurite glass double-cladding fiber. Optics Letters. 2010;**35**:4136-4138. DOI: 10.1364/OL.35.004136

[93] Li LX, Wang WC, Zhang CF, Yuan J, Zhou B, Zhang QY. 2.0 μm Nd^{3+}/Ho^{3+}-doped tungsten tellurite fiber laser. Optical Materials Express. 2016;**6**:2904-2914. DOI: 10.1364/OME.6.002904

[94] Li K, Zhang Q, Fan S, Zhang L, Zhang J, Hu L. Mid-infrared luminescence and energy transfer characteristics of Ho^{3+}/Yb^{3+} codoped lanthanum–tungsten–tellurite glasses. Optical Materials. 2010;**33**:31-35. DOI: 10.1016/j.optmat.2010.07.010

[95] Balaji S, Gupta G, Biswas K, Ghosh D, Annapurna K. Role of Yb^{3+} ions on enhanced ~2.9 μm emission from Ho^{3+} ions in low phonon oxide glass system. Scientific Reports. 2016;**6**:29203. DOI: 10.1038/srep29203

[96] Snyder AW, Love JD. Optical Waveguide Theory. 1st ed. New York: Springer US; 1984. 738 p. DOI: 10.1007/978-1-4613-2813-1

[97] Okamoto K. Fundamentals of Optical Waveguides. 2nd ed. Burlington, MA, USA: Academic Press; 2005. 584 p

[98] Po H, Snitzer E, Tumminelli L, Zenteno L, Hakimi F, Cho NM, Haw T. Double clad high brightness Nd fiber laser pumped by GaAlAs phased array. In: Proceedings of the Optical Fiber Communication Conference; 6-9 February 1989; Houston. OSA; 1989. p. PD7

[99] Akamatsu T. Continuous fabrication of phosphate glass fiber. Journal of Lightwave Technology. 1983;**1**:580-584. DOI: 10.1109/JLT.1983.1072162

[100] Oh K, Paek U-C. Silica Optical Fiber Technology for Devices and Components: Design, Fabrication, and International Standards. 1st ed. Hoboken, NJ, USA: John Wiley & Sons, Inc.; 2012. 472 p.

[101] Roeder E. Extrusion of glass. Journal of Non-Crystalline Solids. 1971;**5**:377-388. DOI: 10.1016/0022-3093(71)90039-1

[102] Roeder E. Flow behaviour of glass during extrusion. Journal of Non-Crystalline Solids. 1972;**7**:203-220. DOI: 10.1016/0022-3093(72)90290-6

[103] Tran DC, Fisher CF, Sigel GH. Fluoride glass preforms prepared by a rotational casting process. Electronics Letters. 1982;**18**:657-658. DOI: 10.1049/el:19820448

[104] Mitachi S, Miyashita T, Kanamori T. Fluoride-glass-cladded optical fibres for mid-infrared ray transmission. Electronics Letters. 1981;**17**:591-592. DOI: 10.1049/el:19810416

[105] Ohishi Y, Sakaguchi S, Takahashi S. Transmission loss characteristics of fluoride glass single-mode fibre. Electronics Letters. 1986;**22**:1034-1035. DOI: 10.1049/el:19860709